A photoemission determination of the band diagram of the Te/CdTe interface

David W. Niles,[a] Xiaonan Li, and Peter Sheldon
National Renewable Energy Laboratory, 1617 Cole Boulevard, Golden, Colorado 80401-3393

Hartmut Höchst
Synchrotron Radiation Center, University of Wisconsin-Madison, 3731 Schneider Drive, Stoughton, Wisconsin 53589-3097

(Received 12 December 1994; accepted for publication 5 January 1995)

Two experiments designed to assist in understanding the physics of certain back contacts on p-type CdTe solar-cell devices are described. In the first experiment, x-ray photoelectron and Auger electron spectroscopies are used to show that etching CdTe in HNO_3:H_3PO_4 results in a Te layer on the CdTe surface. In the second experiment, photoemission spectroscopy is used to explore the electronic properties of evaporated Te deposited on thin-film, polycrystalline p-CdTe in an effort to develop a band diagram for the Te/p-CdTe interface. The motivation for developing the band diagram derives from previous observations that chemically etching polycrystalline p-CdTe solar-cell device material before application of the back contact reduces the series resistance of the device. The key results are that the evaporated Te overlayer is p type and that the valence-band offset between Te and p-CdTe is favorable for low-series-resistance contact, $\Delta E_v = 0.26 \pm 0.1$ eV. © *1995 American Institute of Physics.*

I. INTRODUCTION

CdTe is a favorable semiconductor absorber for thin-film, large-scale photovoltaic (PV) energy collection.[1–3] The highest efficiency attained by a CdTe-based solar cell is ~15.8%.[4] The structure of a typical CdTe-based solar cell consists of a glass superstrate, on which one deposits SnO_2 (front contact), n-type CdS, p-type CdTe, and a back contact. Light impinges on the photocell through the glass superstrate and produces electron-hole pairs in the CdTe. Electrons (holes) flow into (away from) the n-type CdS. Figure 1, in which we list the approximate thickness of the layers, is a schematic of a CdTe-based photocell. We refer to our thin-film, polycrystalline, device-grade p-CdTe simply as thin-film CdTe.

Our experience, as well as the experiences of other researchers, is that applying the back contact to the CdTe is a difficult step in the fabrication process.[5–9] We find that high series resistance associated with the back-contact interface can dominate the series resistance of the device unless we chemically etch the CdTe surface prior to applying the HgTe-graphite back-contact paste.[10–15] In fact, the Fermi levels of many nonreactive metals tend to align near the middle of the optical band gap of CdTe, consistent with charge neutrality or dielectric midgap theories of Schottky-barrier formation.[13,16,17]

Several researches have shown that oxidizing etches, such as mixture of nitric and phosphoric acids, can deplete a crystalline CdTe surface of Cd, thereby creating a Te-rich, strongly p-type layer.[12,14,18] Elemental Te is a degenerate p-type semiconductor with shallow acceptor states within several meV of the valence-band maximum (VBM), no known extrinsic donor states, and a band gap of $E_g = 0.33$ eV at room temperature.[19] In the case of contacts to CdTe solar-cell devices, the presumption is that this degenerate Te back layer is the key to forming the low-resistance contacts. Despite the previous work with Te, we are unaware of an attempt to construct a band diagram for the Te/CdTe interface in an effort to explain why a Te layer might reduce the contact resistance.

We believe that developing a band diagram of the Te/CdTe interface is a prerequisite to understanding how the Te layer on the CdTe surface lowers the resistance. Ideally, we would like to measure the valence-band offset for the Te layer on CdTe created by etching CdTe; however, this process is not amenable to the photoemission technique we have employed to measure valence-band offsets. Therefore, we designed a two-stage experiment: First, we discuss the use of x-ray photoelectron and Auger electron spectroscopies (XPS and AES) to understand the etching process. Then we measured the valence-band offset by vacuum deposition of Te on a sputtered CdTe surface, using ultraviolet photoemission spectroscopy (UPS).

II. EXPERIMENT

We fabricated the CdTe for these experiments at the National Renewable Energy Laboratory (NREL) using closed-space sublimation (CSS). The samples were complete solar-cell structures (without the back contact applied) as shown in Fig. 1. The superstrates we used are SnO_2-coated 7059 glass supplied by Solarex, Inc. Before depositing the CdS we cleaned the superstrates by soaking them for 30 min in an ultrasonically agitated solution of 2% detergent (Contrad CMS-70) in de-ionized water maintained at ~70 °C. After rinsing the substrates for 10 min in de-ionized water, we deposited ~100 nm CdS by solution growth.[20] We then deposited a ~6 μm CdTe thin film on the CdS by CSS, with a source temperature of 630 °C and a substrate temperature of 550 °C in a 10 mTorr pure O_2 ambient. After fabrication we removed the samples from vacuum and exposed them to air. These CSS grown CdTe thin films had dense granular structure with a characteristic grain size of 4 μm.

[a]Electronic mail: david_niles@nrel.gov

 0021-8979/95/77(9)/4489/5/$6.00

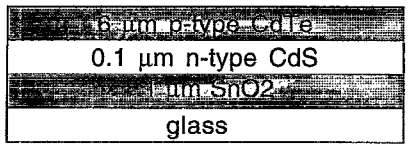

FIG. 1. Schematic of the superstrate structure used for CdS/CdTe-based heterojunction solar cells.

In the first experiment we performed acid etches in a N_2-filled glove box to avoid air contamination. The acid was a concentrated solution of HNO_3 and H_3PO_4. We etched the sample for 1 min, then rinsed them in de-ionized water. After approximately 15 s bubbles formed on the CdTe surface. The acid completely stripped the CdTe and CdS from the glass superstrate in approximately 15 min.

We determined the chemical and compositional quality of the CdTe at NREL using a commercial Physical Electronics 5600 MultiTechnique XPS equipped with Mg anode ($h\nu$ =1253.6 eV) and monochromatized Al anode ($h\nu$=1486.6 eV). We used a spot size of 400 μm, pass energy of 93.90 eV for survey scans, and 5.85 eV for high-resolution scans. We removed surface oxides by sputtering with Ar ions at 3 kV for 1 min at a 2×2 mm raster. We estimated a sputtering rate of 25 nm/min by measuring the depths of sputtered craters, although we did not expect uniform sputtering due to the porous nature of the etched CdTe surfaces.

In the second experiment we performed synchrotron radiation UPS experiments on the formation of the Te/CdTe interface formation at the University of Wisconsin's storage ring Aladdin on the Amoco 6 m toroidal grating monochromator.[21] The experimental apparatus consisted of an angular-resolving hemispherical sector analyzer, an Ar-ion sputter gun, an effusion cell as a source of Te, and a quartz-crystal oscillator to monitor Te depositions. The experimental energy resolution system was 0.10 eV.

After inserting the CdTe thin films into the vacuum system, we sputtered at 3 kV and annealed to 150 °C to remove the contaminants from air exposure. We did not take any precautions to maintain the CdTe at room temperature during Te depositions because the temperature of Te effusion cell was extremely low (~300 °C). A typical evaporation rate was ~5 Å/min. After each Te deposition we measured the Te 4d, Cd 4d, and the valence bands.

III. RESULTS AND DISCUSSION

A. Formation of a Te layer by etching CdTe in HNO_3:H_3PO_4

Figure 2 shows XPS spectra of two CdTe thin films: one that had been etched in the HNO_3:H_3PO_4 (A) etch, and one that had been sputtered in vacuum (B). Compositional analysis of the sputtered sample confirmed stoichiometry, 50 at. % Cd and 50 at. % Te. The sputtering completely removed the common air contaminants, C (E_B=284.5 eV) and O (E_B=531.0 eV), where E_B is the binding energy with respect to the Fermi level.

The surface of the chemically etched sample is nearly devoid of Cd, as one can see from the intensity of the Cd

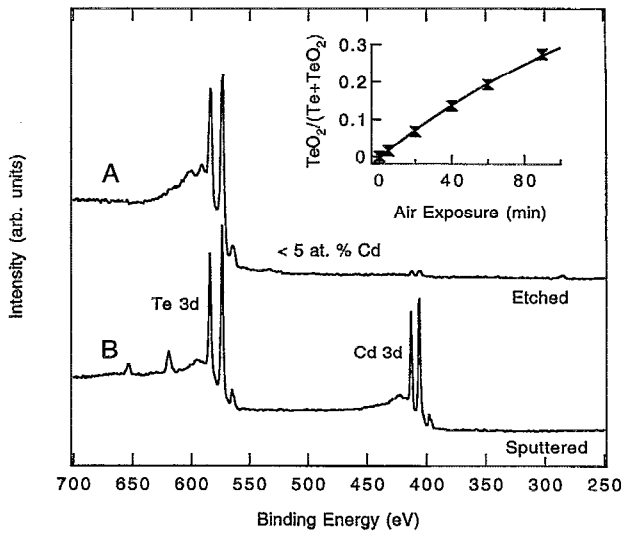

FIG. 2. X-ray photoemission spectrum of a CdTe thin film: (A) dipped in concentrated nitric and phosphoric acids for 1 min and (B) after sputtering at 3 kV. Inset shows rate of oxidation of the Te in air.

signal in spectrum A. By comparing the peak areas in A and B, we determined that the etched sample contained ~5 at. % Cd at the surface. We performed the etch in a N_2-filled glove box and transferred the sample to vacuum without exposure to air. However, the inset shows that short air exposures (~1 min) that would have resulted from performing the etching in air and transferring immediately to the vacuum system would not have resulted in a significant level of O contamination. In a partially oxidized Te thin film the Te 3d shows two distinct components: a Te component at E_B=573.2 eV and a TeO_2 component at E_B=576.8 eV.[12–15] We determined the rate of TeO_2 formation by comparing the areas of the Te and TeO_2 components. After an overnight air exposure, the ratio of oxidized Te to total Te (oxidized plus elemental) was ~61%.

The spectra of Fig. 2 show that the acid etch produces a pure Te layer on the CdTe surface.[10] The compositional profile of Fig. 3 shows the width of the Te layer on the CdTe

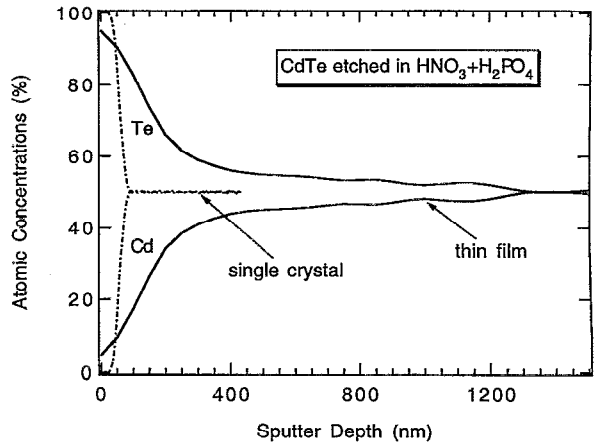

FIG. 3. Sputtering depth profiles for an etched CdTe thin film (solid curves) and single crystal (dotted curves).

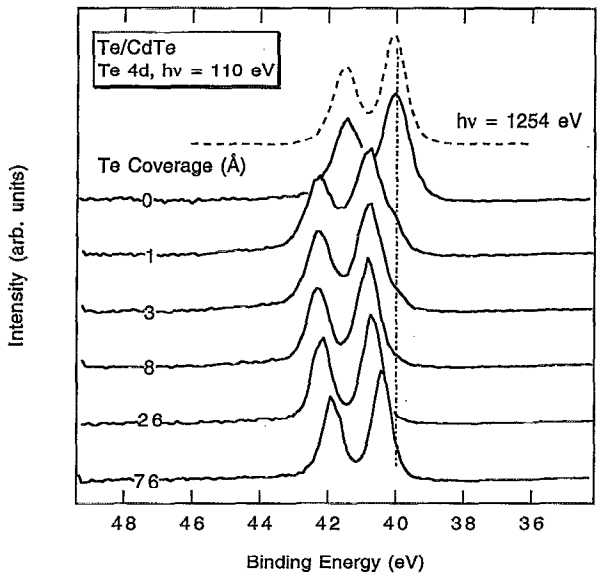

FIG. 4. Photoemission spectra of the Te $3d$ core level taken with $h\nu=110$ eV.

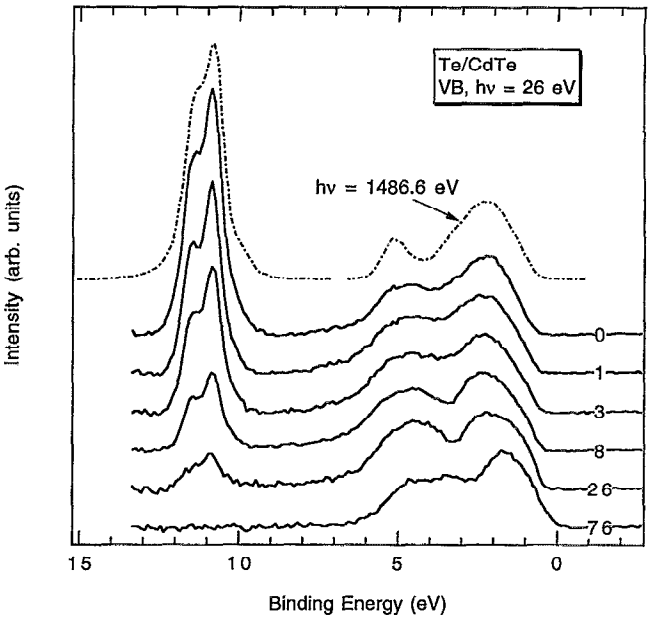

FIG. 5. Photoemission spectra of the valence band and Cd $4d$ core level taken with $h\nu=26$ eV.

substrate.[11] The dotted curves are data from an etched single crystal (100 surface), whereas the solid curves are from an etched, polycrystalline thin film.[10–15] The etched single crystal has a pure Te layer of width ~30 nm, followed by a transition region of increasing Cd concentration. The single crystal is stoichiometric at a depth of 80 nm. The width of the transition region from a pure Te layer on the single crystal to stoichiometric CdTe is ~50 nm, which is much larger than the depth resolution of the sputter profile (~10 nm, as determined from atomically abrupt layered III-V superlattices grown by metal oxide chemical-vapor deposition).[22]

The depth profile of the polycrystalline thin film is remarkably different. The surface is not completely devoid of Cd, the transition region from the surface composition to stoichiometry is nearly 1500 nm, and the composition has a plateau between 500 and 1200 nm. These differences are a combined manifestation of the initial surface roughness of the Te layer (700 nm, as measured with a DekTak) and an enhanced etching rate along grain boundaries of the polycrystalline CdTe.

B. Simulating the etched layer by vacuum deposition of Te

Figures 4–7 show an UPS analysis of Te layers deposited by vacuum evaporation on a CdTe thin film. The CdTe thin film used for the simulated Te layer is a second piece from the same sample used in our work on the HNO_3:H_3PO_4 etch. Figure 4 shows UPS spectra of the Te $4d$ core level. The dotted curve is the Te $4d$ taken with monochromatized Al$K\alpha$ radiation on the Physical Electronics 5600 XPS MultiTechnique system. It is the same sample as shown in curve B of Fig. 2. The solid curves are from a different piece of that same CdTe thin film that we studied at Aladdin.

Before any Te evaporation, we observe well-resolved $j=5/2$ and $j=3/2$ components to the Te $3d$. Fitting with a pair of Voigt doublets yields a spin-orbit splitting of 1.46 eV, a full width at half-maximum (FWHM) of 0.46 eV, and a Gaussian/Lorentzian ratio of 0.7 (i.e., 70% Gaussian).[23] The binding energy of the 5/2 component is $E_B=40.02$ eV. With the addition of 1 Å Te, the line shape changes to a pair of doublets where the $j=5/2$ components have binding energies of $E_B=40.05$ eV and $E_B=40.80$ eV. With increasing coverage the intensity of the doublet at higher binding energy increases and shifts slightly to $E_B=40.70$ eV for a coverage of 26 Å, whereas the intensity of the doublet at lower binding energy decreases and disappears entirely at a coverage of 8 Å. Increasing the coverage from 26 to 76 Å leads to an abrupt binding energy shift of the higher doublet from $E_B=40.70$ eV to $E_B=40.40$ eV.

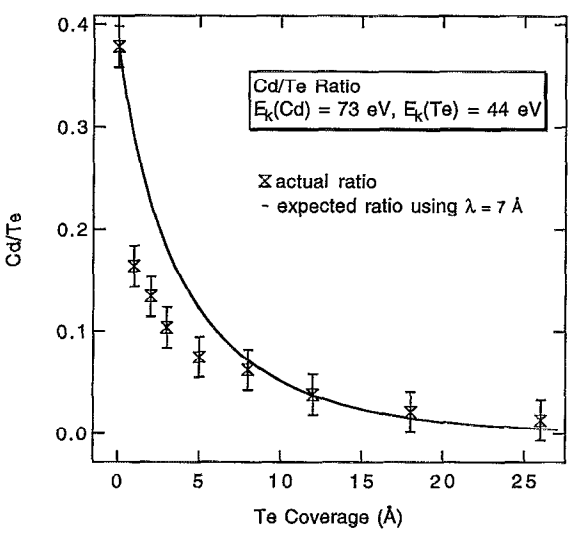

FIG. 6. Ratio of the Cd $4d$ peak area to the Te $4d$ peak area as a function of Te thickness.

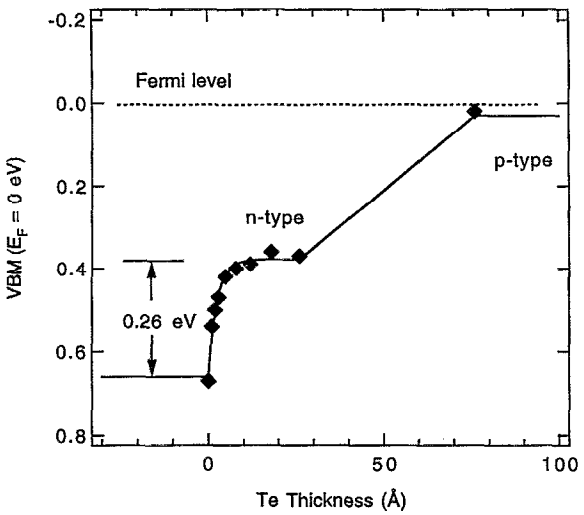

FIG. 7. Position of the valence-band maximum as a function of Te overlayer thickness.

Figure 5 shows the corresponding spectra of the Cd $4d$ and valence band. The dotted curve shows the valence band and Cd $4d$ taken with monochromatized Al$K\alpha$ radiation. With increasing Te coverage the intensity of the Cd $4d$ core emission decreases, but the energy does not shift. The valence emission takes on increasing Te character with increasing Te coverage. We determined the position of the VBM by linearly extrapolating the leading edge of the valence-band emission.

The following picture emerges: On the pristine surface, electronic states pin the Fermi level at approximately the middle of the CdTe band gap. As one sees by the position of the VBM and the immovability of the Cd $4d$ in Fig. 5, the position of the CdTe valence bands with respect to the Fermi level do not change with coverage. With the first evaporation of 1 Å Te, a second doublet of the Te $4d$ emerges and is even stronger than the CdTe doublet seen in the spectrum without any Te. Between coverages of 1 Å Te and ~8 Å Te, we observe two Te $4d$ doublets corresponding to two different bonding configurations for the Te: a Cd—Te bond whose $j=5/2$ component has $E_B=40.05$ eV, and a Te—Te bond whose $j=5/2$ component has $E_B=40.80$ eV. The Cd—Te bonds emanate from CdTe, whereas the Te—Te bonds emanate from the Te overlayer.

Up to a coverage of 26 Å the Te overlayer is n type, contradictory to the observation that no known donors exist for Te.[19] However, defect levels in the CdTe dominate the conductivity type at the surface region, and the Debye length is simply longer than the thickness of the Te. The Te overlayer becomes p type at a coverage of 76 Å, when the acceptor levels in the Te layer dominate the conductivity type. The band gap of Te is $E_g=0.33$ eV, and the change in binding energy of the Te $4d$ is $\Delta E_B=0.3$ eV between 26 and 76 Å Te. The change in conductivity type accounts for the change in binding energy of both the VBM and the Te $4d$ between a coverage of 26 and 76 Å.

The perplexing property of the formation of the Te/CdTe interface is the drastic decrease in the CdTe component of the Te $4d$ with only 1 Å Te. Figure 6 shows the ratio of the Cd $4d$ peak area to the Te $4d$ peak area as a function of the Te overlayer thickness. For a continuous, nongranular coverage model without any intermixing at the interface or redistribution of the CdTe substrate, the Cd $4d$ intensity would decrease as $\mathrm{Cd}=\mathrm{Cd}_0\exp(-x/\lambda)$, where Cd_0 is the intensity before Te deposition and λ is the photoelectron escape depth. The Te intensity would increase approximately as $\mathrm{Te}=\mathrm{Te}_0[2-\exp(-x/\lambda)]$, where Te_0 is the intensity before Te deposition. Although the Cd and Te should have different escape depths, we may set them both equal to 7 Å in this model because they both fall near the minimum of the universal escape depth curve.[24] The solid curve in Fig. 6 is the expected ratio of the Cd $4d$ to Te $4d$ as a function of thickness using this simple model.

For Te coverages below 8 Å, the actual ratio is approximately half of the expected ratio. The unexpected, rapid attenuation is not an artifact of underestimating the Te thickness, as we proved by repeating the experiment while paying particular attenuation to the peak heights. The first coverages of Te cause a redistribution of atoms at the CdTe surface that accentuates emission from Te—Te bonds at the expense of Cd—Te bonds. We took the zero-Te thickness data only after a light sputter at room temperature to remove air contaminants (~30 Å). Because the temperature of the Te effusion cell is only 300 °C, and because the effusion cell is 15 cm from the sample, the sample temperature does not rise from radiative heating during evaporation. The redistribution mechanism, although beyond the scope of this article, is not related to heating.

Figure 7 shows the position of the VBM as a function of Te overlayer thickness. For Te coverages between 1 and 5 Å we observe a sharp increase in the VBM as the valence-band emission adopts increasingly more Te character, and a plateau between 8 and 26 Å coverage. The beginning of the plateau (8 Å) corresponds to the disappearance of the Cd—Te bonds in Fig. 4. In this plateau, we see the VBM of n-type Te. Taking the band gap of Te to be $E_g=0.33$ eV puts the conduction-band minimum (CBM) slightly below the Fermi level, although the accuracy of the leading edge technique for determining the VBM is only ± 0.05 eV. Therefore, we conclude that the Te is strongly n type and the Fermi level is very close to the CBM for coverages below 26 Å.

At a coverage of 76 Å the Te conductivity switches abruptly from n to p type, seen by the 0.35 eV decrease in the binding energy of the VBM (Fig. 5) and the 0.30 eV decrease in binding energy of the Te $4d$ (Fig. 4). Unfortunately we could not observe the Cd $4d$ core-level emission at a coverage of 76 Å, and do not know whether the CdTe bands moved with the Te bands.

There are four distinct regions with Te thickness. The first region is at no coverage where one sees the VBM of CdTe; the second region covers the thickness range between 1 and 8 Å, where one sees the emergence of the Te VBM; the third region is simply n-type Te; and the fourth region is the final coverage and is p-type Te. Further deposition would only increase the thickness of the p-type Te layer but not produce any more insight into the electronic properties of the Te/CdTe interface.

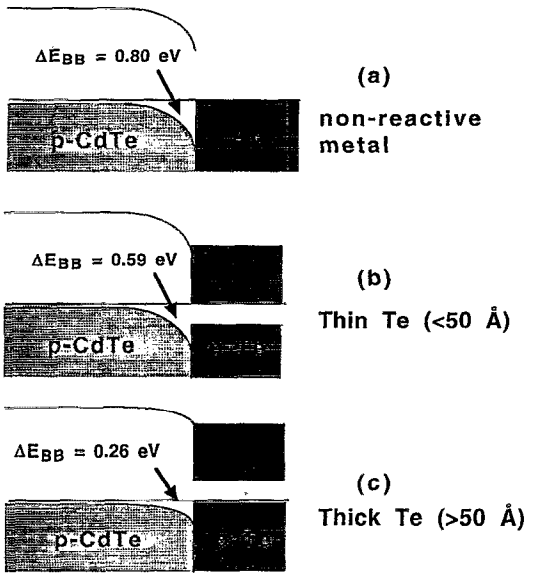

FIG. 8. Proposed explanation for why p-type Te may make a better contact to CdTe than many nonreactive metals.

The band gap of Te is E_g=0.33 eV, and we observe $E_{VBM}-E_F$=0.38±0.05 eV at a coverage of 26 Å, and $E_{VBM}-E$=0.03±0.05 eV at a coverage of 76 Å.[19] The position of the Te VBM with respect to the Cd VBM gives the valence-band offset, ΔE_v=0.26 eV. The observed p-type conductivity in the CdTe would favor PV performance.

Although the valence-band offset between Te and CdTe is a sizable fraction of the Te band gap [ΔE_v=0.26±0.1 eV, whereas E_g(Te)=0.33 eV], the electronic structure of the Te/CdTe heterojunction may be much more favorable to hole flow than the electronic structure of many metal/CdTe interface. We propose that the strong p-type character of the Te and not the band lineup is the reason Te makes a good back contact. In panel (a) of Fig. 8, we show a diagram of the Au/p-CdTe Schottky barrier drawn from the data of Ref. 5. We assume that the Fermi level is at the VBM in the bulk of the p-type CdTe thin film only for the purpose of drawing the diagram. Metals such as Au that pin the interface Fermi level near the middle of the p-type CdTe band gap will not make good back contacts because holes will feel the electric field that accompanies the band bending.

We find that the clean CdTe surface has the Fermi level pinned near the middle of the band gap, as seen in Fig. 7. Thin Te layers (<50 Å) have insufficient doping levels to overpower the pinned position of the Fermi level, so that the electronic structure appears as in panel (b) of Fig. 8. We draw the Te bands flat because they are thin and have relatively large conductivity compared to CdTe. For thick Te layers (>50 Å), the strong p-type character of the Te overlayer takes over, and moves the Fermi level to the bottom of the Te band gap as seen in panel (c) of Fig. 8. The CdTe bands must move with the Te band to maintain the valence-band offset. This movement flattens the CdTe bands from bending 0.8 eV for a Au contact to only 0.26 eV for a Te contact, improving hole flow. We have not yet proven this picture, but we contend that it is consistent with our data on the Fermi-level position.

Finally, we would like to propose vacuum evaporation as an alternative method of producing a Te layer on the CdTe. Vacuum evaporation and etching CdTe may produce an entirely different Te layer on the CdTe surface, and the etched layer may have a unique feature that facilitates lowering the resistance. In fact, Tyan has stated that vacuum evaporation of Te is an unsuitable method for producing low-resistance contact.[25] In light of the band structure, we believe vacuum evaporation needs further consideration. It voids the use of acids and the creation of shunting resistance problems, it is amenable to the CSS fabrication process, and it has a reasonable valence-band offset.

ACKNOWLEDGMENTS

The National Science Foundation funds the Synchrotron Radiation Center. The authors would like to thank the staff of the Synchrotron Radiation Center for technical assistance during the experiments and also T. Gessert of NREL for critically reading the manuscript. We performed this work under DOE Contract No. DE-AC36 B CH10093.

[1] C. Ferekides, in Proceedings of the 12th European Photovoltaic Solar Energy Conference, Amsterdam, April 1994.
[2] T. L. Chu and S. S. Chu, Prog. Photovoltaics **1**, 31 (1993).
[3] Y.-S. Tyan, Sol. Cells. **23**, 19 (1988).
[4] M. A. Green and K. Emery, Prog. Photovoltaics **2**, 231 (1994).
[5] D. J. Friedman, I. Lindau, and W. E. Spicer, Phys. Rev. B **37**, 731 (1988).
[6] A. L. Fahrenbruch, Sol. Cells **21**, 399 (1987).
[7] J. P. Ponpon, Solid-State Electron. **28**, 689 (1985).
[8] R. H. Williams, N. Forsyth, I. M. Dharmadasa, and Z. Sobiesierski, Appl. Surf. Sci. **41/42**, 189 (1989).
[9] D. Rioux, D. W. Niles, and H. Höchst, J. Appl. Phys. **73**, 8381 (1993).
[10] W. J. Danaher, L. E. Lyons, and G. C. Morris, Appl. Surf. Sci. **22/23**, 1083 (1985).
[11] W. J. Danaher, L. E. Lyons, M. Marychurch, and G. C. Morris, Appl. Surf. Sci. **27**, 338 (1986).
[12] A. J. Ricco, H. S. White, and M. S. Wrighton, J. Vac. Sci. Technol. A **2**, 910 (1984).
[13] I. M. Dharmadasa, A. B. McLean, M. H. Patterson, and R. H. Williams, Semicond. Sci. Technol. **2**, 404 (1987).
[14] H. S. White, A. J. Ricco, and M. S. Wrighton, J. Phys. Chem. **87**, 5140 (1983).
[15] S. Tanaka, J. Bruce, and M. S. Wrighton, J. Phys. Chem. **85**, 3778 (1981).
[16] M. Cardona and N. E. Christiensen, Phys. Rev. B **35**, 6182 (1987).
[17] W. A. Harrison and J. Tersoff, J. Vac. Sci. Technol. B **4**, 1068 (1986).
[18] F. Debbagh, H. Muhssine, E. L. Ameziane, M. Azizan, and M. Brunel, Sol. Energy Mater. Sol. Cells **31**, 1 (1993).
[19] O. Madelung, M. Schultz, and H. Weiss, in *Semiconductors*, Group III: Crystal and Solid State Physics, Vol. 17, Landoldt-Börnstein New Series, *Numerical Data and Functional Relationships in Science and Technology*, edited by K.-H. Hellwege (Springer, Berlin, 1983), pp. 106–117.
[20] L. Stolt, J. Hedstrom, J. Kessler, M. Ruckh, K. Velthaus, and H. Schock, Appl. Phys. Lett. **62**, 597 (1993).
[21] D. C. Mancini, M. Bissen, D. Rioux, R. Patel, G. Rogers, E. L. Brodsky, and H. Höchst, Rev. Sci. Instrum. **63**, 1269 (1992).
[22] The authors would like to thank M. Wanlass of the National Renewable Energy Laboratory for reference III-V superlattices.
[23] P. M. A. Sherwood, in *Practical Surface Analysis by Auger and X-ray Photoelectron Spectroscopy*, edited by D. Briggs and M. P. Seah (Wiley, New York, 1984), p. 459.
[24] S. Tanuma, C. J. Powell, and D. R. Penn, Surf. Interface Anal. **13**, 911 (1991).
[25] Y.-S. Tyan, U. S. Patent No. 4,319,069 (9 March 1982).